

Finite element network approximation of conductivity in particle composites

Daniel Peterseim · Carsten Carstensen

Received: 29 November 2010 / Revised: 30 August 2012 / Published online: 21 October 2012
© Springer-Verlag Berlin Heidelberg 2012

Abstract A new finite element method computes conductivity in some unstructured particle-reinforced composite material. The 2-phase material under consideration is composed of a poorly conducting matrix material filled by highly conducting circular inclusions which are randomly dispersed. The mathematical model is a Poisson-type problem with discontinuous coefficients. The discontinuities are huge in contrast and quantity. The proposed method generalizes classical continuous piecewise affine finite elements to special computational meshes which encode the particles in a network structure. Important geometric parameters such as the volume fraction are preserved exactly. The computational complexity of the method is (almost) proportional to the number of inclusions. This is minimal in the sense that the representation of the underlying geometry via the positions and radii of the inclusions is of the same complexity. The discretization error is proportional to the distance of neighboring inclusions and independent of the conductivity contrast in the medium.

Mathematics Subject Classification (2000) 65N15 · 65N30 · 74Q20

The work of D. Peterseim was supported by the DFG Research Center Matheon Berlin through project C33.

D. Peterseim (✉) · C. Carstensen
Institut für Mathematik, Humboldt-Universität zu Berlin,
Unter den Linden 6, 10099 Berlin, Germany
e-mail: peterseim@math.hu-berlin.de

C. Carstensen
Department of CSE, Yonsei University, Seoul, Korea

1 Introduction

Composite materials (or *composites* for short) are engineered materials made from two or more constituents with significantly different physical properties. In a typical configuration, randomly distributed filler particles (inclusions) are surrounded by a second material (matrix) which binds the filler particles together.

The numerical simulation of material properties aims at a better understanding how conductivity depends on controllable variables (e.g., thermal conductivities of the material components, relative volumes, and particles shapes) and hence provides the opportunity to develop materials with enhanced performance for the particular application.

The design of efficient and reliable numerical methods for such problems is challenging. The complexity of the underlying geometry makes classical approaches hardly feasible (cf. Sect. 1.2); in the typical geometric setting, the inclusions are too big for any perturbation analysis or homogenization method, and they are too many or they are packed too densely to resolve them easily with standard finite element meshes. We face this difficulty even for simple continuum models of some material property of interest, e.g. the linear elliptic model problem of heat conduction considered in this paper (see Sect. 1.1).

Based on an efficient treatment of the microscopic geometry, the new method described in this paper (cf. Sect. 1.3) allows reliable numerical simulation of the model problem with many inclusions independent of the degree of disorder in the geometry.

1.1 Model problem

This paper considers a representative 2-dimensional model of a particle-reinforced composite occupying the nonempty open bounded convex polyhedral domain $\Omega \subset \mathbb{R}^2$. Let \mathcal{B}_{inc} be a set of closed, pairwise disjoint disks of positive radii (inclusions) contained in a domain $\Omega \subset \mathbb{R}^2$, i.e.,

$$B \subset \Omega \quad \text{and} \quad \text{dist}(B, \tilde{B}) > 0 \quad \text{for all } B, \tilde{B} \in \mathcal{B}_{\text{inc}} \text{ with } B \neq \tilde{B}. \quad (1.1)$$

In the present context, the number $N := \#\mathcal{B}_{\text{inc}}$ of inclusions is a very large parameter. The two material phases are represented by the union of the inclusions Ω_{inc} , and by the so called matrix (the perforated domain) Ω_{mat} ,

$$\Omega_{\text{inc}} := \bigcup_{B \in \mathcal{B}_{\text{inc}}} \text{int}(B) \quad \text{and} \quad \Omega_{\text{mat}} := \Omega \setminus \overline{\Omega}_{\text{inc}}.$$

The outer boundary $\Gamma := \partial\Omega$ is partitioned into two parts Γ_D and Γ_N , where Γ_D is closed and has a positive surface measure while its relative complement $\Gamma_N := \Gamma \setminus \Gamma_D$ is relatively open, and the number of contact points $\Gamma_D \cap \overline{\Gamma}_N$ is finite.

The material geometry enters the problem through a coefficient function $c \in L^\infty(\Omega)$ which jumps between the material components. For simplicity c is chosen to

be constant with respect to each of the two phases and normalized with respect to the matrix material, i.e.,

$$c(x) = \begin{cases} 1 & \text{if } x \in \Omega_{\text{mat}}, \\ c_{\text{cont}} & \text{if } x \in \Omega_{\text{inc}}. \end{cases} \tag{1.2a}$$

The constant $c_{\text{cont}} \geq 1$ represents the conductivity contrast in the medium.

Consider the set of admissible temperature distributions

$$\mathcal{A} := u_D + V \text{ with } V := \{u \in H^1(\Omega) \mid u = 0 \text{ on } \Gamma_D\} \tag{1.2b}$$

for $u_D \in H^1(\Omega) \cap C^0(\overline{\Omega})$. Given some force density $f \in V^*$, the effective conductivity of the composite

$$c_{\text{eff}} := \min_{u \in \mathcal{A}} \mathfrak{E}(u) \tag{1.2c}$$

minimizes the energy functional \mathfrak{E} ,

$$\mathfrak{E}(v) := \frac{1}{2} \int_{\Omega} c(x) |\nabla v(x)|^2 dx - \int_{\Omega} f(x)v(x) dx \text{ for all } v \in H^1(\Omega). \tag{1.2d}$$

1.2 Challenges to numerical simulations

In practical applications, the parameter $c_{\text{cont}} \gg 1$ is very large. In addition, the coefficient function, which is the output of certain (random) production processes (e.g. mixing of the particles within a liquid matrix material followed by hardening), has to be regarded as a statistical parameter. Corresponding to Berlyand [3], the latter two issues, random micro-structures on multiple scales and high contrast in physical properties, are the two characteristic features of general composites. They lead to major difficulties for a numerical approximation of problem (1.2).

Classical FEM A classical method for the approximate solution of (1.2) is the finite element method. However, in the present context, standard finite element approaches suffer from the fact that the material interface $\partial\Omega_{\text{inc}}$ needs to be resolved by the underlying mesh in order to get satisfactory results. The required resolution of the coefficient geometry forces even the coarsest available meshes to be very fine, i.e., the minimal mesh size has to be at most of order of the inclusion radii. Additionally, finite element methods often require high quality meshes (shape regularity) which puts even more constraints on mesh generation. Thus, the minimal number of nodes in a reasonable mesh depends critically on the distribution of the holes and their distances; Fig. 1 illustrates the problem in a model situation, which is eased for visualization purposes.

Minimal complexity Since the underlying geometry is of stochastic nature problem (1.2), typically, needs to be solved many times for different coefficient configurations

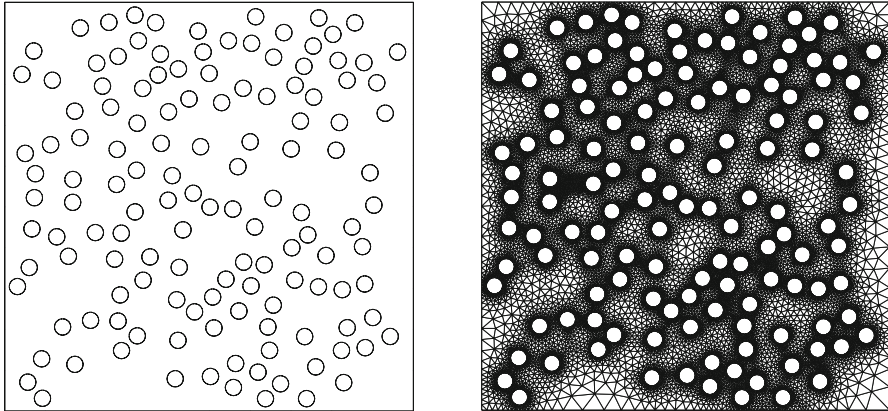


Fig. 1 Model domain (unit square) containing 133 circular inclusions with radius $r = 0.02$ (left) and “coarse” shape regular triangulation with 33903 elements (right)

within a statistical investigation of material properties (by a Monte Carlo method). For example, the accuracy of the approximation of the expected temperature distribution subject to a random distribution of particles in the material, is of order $M^{-1/2}$, where M denotes the number of samples. Since the coefficient is different for different samples, meshes cannot be re-used but need to be re-computed for every single sample of the particle distribution. Hence, the computation of the finite element mesh is crucial in all complexity discussions and cannot be neglected as a precomputation (cf. Fig. 1). With regard to the possibly huge number of instances of problem (1.2) that need to be considered, this paper aims at a reasonable discrete model of minimal complexity. Minimality is determined by the data of the problem and therefore mainly by its geometry. The geometry representation requires storing the pairs of centers and radii of the N inclusions (the complexity of the representation of the outer boundary is supposed to be small compared to N). A model is considered to have minimal complexity if it provides an approximate solution in time and space complexity $\mathcal{O}(N)$. The finite element method to be presented in this paper satisfies the complexity requirement up to logarithmic factors (cf. Section below).

1.3 The new structural finite element approach

In this paper ideas from network approximations [3–5, 19] are combined with non-standard finite element methods to derive a new structural finite element method of almost minimal complexity. In particular, a special geometry treatment inspired by networks is combined with the flexibility of finite element methods. As in discrete network methods, the inclusions are modeled in a network structure. They appear as elements of the computational mesh, supplemented by channel-like objects that connect neighboring inclusions and, finally, triangles. The mesh generalizes standard Delaunay triangulations of points in the plane to sets of disks. It can be computed and represented efficiently. A generalization of continuous first-order finite ele-

ments based on the new, problem-adapted subdivisions is introduced. Its realization is conceivably simple and it provides accurate numerical approximations at almost minimal complexity. More precisely, for the solution $u \in \mathcal{A} \cap H^2(\Omega_{\text{mat}} \cup \Omega_{\text{inc}})$ of (1.2) and its structural finite element approximation u_S it holds (see Theorem 3.1, Corollaries 3.1 and 3.2).

$$\|\sqrt{c}\nabla(u - u_S)\|_{L^2(\Omega)} \leq C_{f,u_D,\mathcal{B}_{\text{inc}}} \|h\|_{L^\infty(\Omega)},$$

where h is a local mesh size parameter. The constant does *not* depend on contrast. Its dependencies on the geometry of the material (e.g., touching inclusions) are discussed in detail.

The overall motivation for the novel network approximation is its optimal complexity in the sense that the cost for a meaningful approximation remains proportional to the number of inclusions.

1.4 Numerical upscaling

The number of degrees of freedom might be reduced further by using multiscale methods, e.g., [7, 11, 16, 17, 20, 21]. These methods are based on arbitrary coarse meshes that, more or less, ignore the geometric scales of the coefficient. The influence of the coefficient is instead coded in the finite element basis functions or some modified discrete operator. For this, multiscale methods require some preprocessing that involves the solution of the original problem on subdomains. The solution of these local problems, however, faces the same difficulties as the original problem, i.e., it requires submeshes fine enough to capture the heterogeneities (the influence of the microscopic geometry on macroscopic material properties can only be studied if the microscopic geometry enters the discretization). In this regard, the method presented here might be employed as an efficient fine scale solver within some multiscale numerical framework.

1.5 Outline

Section 2 defines a problem adapted generalization of triangular meshes modeling the inclusions as (vertex-like) elements of a subdivision. Based on this new type of meshes a generalized nodal basis defining a generalized conforming first-order approximation space is introduced. Contrast-independent a priori error estimates for the proposed new finite element method are given in Sect. 3. Section 4 discusses open problems and future generalizations of the method.

1.6 Notation

In this paper, capital letters A, B, C, \dots indicate sets. Calligraphic capital letters $\mathcal{B}, \mathcal{P}, \dots$ denote sets of sets. For a given set of sets \mathcal{B} the union of its elements is denoted by $\cup \mathcal{B} := \bigcup_{B \in \mathcal{B}} B$. Basic topological notations are used: For any subset X

of a metric space its closure is denoted by \overline{X} , its interior by $\text{int}(X)$, and its boundary by $\text{bnd}(X)$. In what follows, $\text{dist}(\cdot, \cdot)$ denotes the Euclidean distance in \mathbb{R}^2 . The measure $|\cdot|$ is context-sensitive and refers to the volume of a set relative to its dimension, i.e., $|\cdot|$ denotes the length of a curve, or the area of a domain. The distance between nonempty subsets $A, B \subset \mathbb{R}^2$ reads

$$\text{dist}(A, B) := \inf_{x \in A, y \in B} \text{dist}(x, y). \quad (1.3)$$

Given some bounded domain Ω , standard notation for (fractional) Sobolev spaces $W_p^m(\Omega)$, $m \geq 0$, $p \in \mathbb{N} \cup \{0\}$, and their corresponding norms $\|\cdot\|_{W_p^m(\Omega)}$ and seminorms $|\cdot|_{W_p^m(\Omega)}$ is used; $H^m(\Omega)$ abbreviates $W_2^m(\Omega)$ ($m \in \mathbb{N}$) and $L^p(\Omega)$ abbreviates $W_p^0(\Omega)$. Given two disjoint bounded Lipschitz domains Ω_1 and Ω_2 , the space $H^m(\Omega_1 \cup \Omega_2)$ denotes the space of all functions $u \in L^2(\Omega_1 \cup \Omega_2)$ with $u|_{\Omega_1} \in H^m(\Omega_1)$ and $u|_{\Omega_2} \in H^m(\Omega_2)$. The dual space of a Hilbert space V is indicated by V^* . The space of \mathbb{R} -valued continuous functions on a set Ω is denoted by $C^0(\Omega)$.

2 A minimal conforming finite element space

This section introduces a conforming finite element space which can be regarded as a generalization of the classical continuous piecewise affine finite element space on a special mesh.

2.1 Geometric preliminaries

Cyclic polygons A convex polygon T is the closed convex hull of 2 or more distinct points. The set of vertices (corners) $\mathcal{V}(T)$ is the minimal set of points $x_1, x_2, \dots, x_k \in \mathbb{R}^2$, such that $T = \text{conv}(\{x_1, x_2, \dots, x_k\})$. According to the number of its vertices, a convex polygon is denoted as a convex k -gon. The boundary of a convex k -gon can be described by the union of at most k line segments called *edges*. The set of edges of a convex polygon T is denoted by $\mathcal{E}(T)$. A convex polygon T is called *cyclic* if its vertices (corners) $\mathcal{V}(T)$ are located on the boundary of a (closed) disk $CD = CD(T)$ which is denoted as the *circumdisk* of T . Examples of cyclic polygons are line segment, triangles, or rectangles.

Infinite Delaunay Triangulations A regular (possibly infinite) triangulation of a domain $\Omega \subset \mathbb{R}^2$ into cyclic polygons is a set of cyclic polygons T such that

$$\cup T = \overline{\Omega}$$

and any two distinct cyclic polygons are either

- disjoint, $T_1 \cap T_2 = \emptyset$, or
- share exactly one vertex z , $T_1 \cap T_2 = \mathcal{V}(T_1) \cap \mathcal{V}(T_2) = \{z\}$, or
- have one edge $E = \text{bnd}(T_1) \cap \text{bnd}(T_2) = \mathcal{E}(T_1) \cap \mathcal{E}(T_2)$ in common.

The set of all edges resp. vertices of a triangulation \mathcal{T} is written as

$$\mathcal{E}(\mathcal{T}) := \bigcup_{T \in \mathcal{T}} \mathcal{E}(T) \quad \text{resp.} \quad \mathcal{V}(\mathcal{T}) := \bigcup_{T \in \mathcal{T}} \mathcal{V}(T).$$

A regular triangulation \mathcal{T} is called *Delaunay* [10] if every element $T \in \mathcal{T}$ satisfies the Delaunay criterion

$$CD(T) \cap \mathcal{V}(\mathcal{T}) = \mathcal{V}(T), \tag{2.1}$$

that is, the circumdisc of T does not contain any vertices of \mathcal{T} except those of T . Given a set of vertices \mathcal{V} , the Delaunay triangulation of $\text{conv}(\mathcal{V})$ is uniquely determined (if cyclic polygons are considered). It can be constructed, e.g., by exploiting duality with respect to the Voronoi diagram [27] of \mathcal{V} . The uniqueness is due to the consideration of cyclic polygons instead of just triangles. In the subsequent paragraph, cyclic k -gons with $k > 3$ will further be decomposed into triangles.

2.2 Geometric modeling of particle composites

The geometry of model problem (1.2) is represented by a finite set \mathcal{B} of closed disks. Every $B \in \mathcal{B}$ is described by its center $c_B = \text{mid}(B)$ and its radius $r_B = \text{diam}(B)/2 \geq 0$. The elements of \mathcal{B} are denoted as *generalized vertices* and partitioned into the two subsets \mathcal{B}_{inc} and \mathcal{B}_{mat} , i.e.,

$$\mathcal{B} = \mathcal{B}_{\text{inc}} \cup \mathcal{B}_{\text{mat}} \quad \text{and} \quad \mathcal{B}_{\text{inc}} \cap \mathcal{B}_{\text{mat}} = \emptyset.$$

The set \mathcal{B}_{inc} contains the inclusions of model problem (1.2), i.e., closed disks of positive radius. The set \mathcal{B}_{mat} contains closed disks of radius zero with

$$\text{conv}(\cup \mathcal{B}_{\text{mat}}) = \overline{\Omega} \quad \text{and} \quad \Gamma_D \cap \overline{\Gamma}_N \subset \cup \mathcal{B}_{\text{mat}}.$$

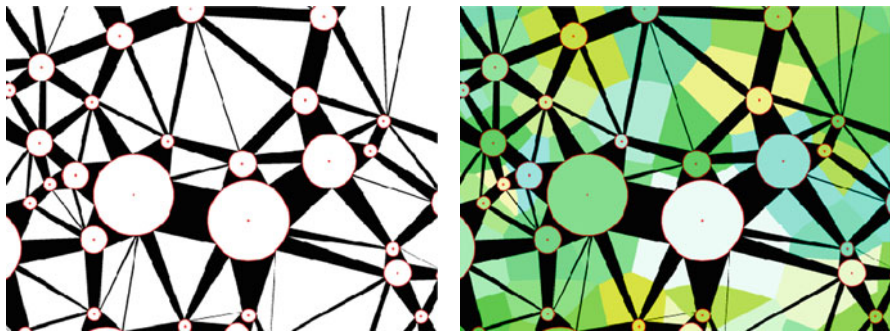
Thus \mathcal{B}_{mat} contains the corners of $\partial\Omega$ and all points where the type of boundary condition switches between Dirichlet and Neumann; but \mathcal{B}_{mat} might contain additional points (disks with vanishing radii) in the interior of the matrix Ω_{inc} , which offers the possibility of refinement and increased local resolution within the finite element framework.

By \mathcal{T}_{mat} we denote the Delaunay triangulation of Ω_{mat} such that

$$\mathcal{V}(\mathcal{T}_{\text{mat}}) = \mathcal{B}_{\text{mat}} \cup \bigcup_{B \in \mathcal{B}_{\text{inc}}} \partial B.$$

Figure 2 displays a detail of \mathcal{T}_{mat} for some set of disks \mathcal{B} . Obviously, \mathcal{T}_{mat} consists of two classes of cyclic polygons (see [24]), namely,

- a) (possibly infinitely many) cyclic 2-gons $\mathcal{T}_{\text{mat}}^{\mid}$, i.e., line segments whose vertices are located on the circumference of exactly two distinct disks, and



(a) Generalized Delaunay triangulation

(b) Generalized Delaunay triangulation and dual Voronoi tessellation

Fig. 2 Generalized Delaunay triangulation with respect to disks in the plane

b) (finitely many) cyclic k -gons $\mathcal{T}_{\text{mat}}^\Delta$ for $k \geq 3$.

For simplicity we assume that $\mathcal{T}_{\text{mat}}^\Delta$ contains exclusively triangles. This assumption can always be fulfilled if we consider a triangulation $\tilde{\mathcal{T}}_{\text{mat}}$ in which the 4, 5, ... -gons of \mathcal{T}_{mat} are further decomposed into triangles; $\tilde{\mathcal{T}}_{\text{mat}}$ is not Delaunay in the sense of (2.1) but fulfills the weaker Delaunay criterion

$$\text{int}(CD(T)) \cap \mathcal{V}(\tilde{\mathcal{T}}_{\text{mat}}) = \emptyset \quad \text{for all } T \in \tilde{\mathcal{T}}_{\text{mat}}, \tag{2.2}$$

that is, there are no vertices of $\tilde{\mathcal{T}}_{\text{mat}}$ in the interior of the circumdisk of $T \in \tilde{\mathcal{T}}_{\text{mat}}$. The subset $\mathcal{T}_{\text{mat}}^\Delta$ of triangles of \mathcal{T}_{mat} provides structural (combinatorial) information about the set of inclusions \mathcal{B}_{inc} . It induces a neighborhood relation $\mathcal{N} \subset \mathcal{B}_{\text{inc}} \times \mathcal{B}_{\text{inc}}$ defined by the rule: $(B_1, B_2) \in \mathcal{N}$ if there exists a $T \in \mathcal{T}_{\text{mat}}^\Delta$ such that $V(T) \subset B_1 \cup B_2$ and $V(T) \cap B_1 \neq \emptyset$ and $V(T) \cap B_2 \neq \emptyset$. For every pair $(B_1, B_2) \in \mathcal{N}$ of neighboring disks we define the channel-like object (a bundle of line segments)

$$E(B_1, B_2) := \cup\{T \in \mathcal{T}_{\text{mat}} : V(T) \subset B_1 \cup B_2\}.$$

Since $E(B_1, B_2)$ is an object that connects exactly two generalized vertices (disks) we denote $E(B_1, B_2)$ a generalized edge.

A finite subdivision \mathcal{G} of Ω , which will serve as the finite element mesh later, is given by

$$\mathcal{G} = \mathcal{B}_{\text{inc}} \cup \mathcal{E} \cup \mathcal{T},$$

where \mathcal{B}_{inc} is the given set of disks, $\mathcal{E} := \{E(B_1, B_2) : (B_1, B_2) \in \mathcal{N}\}$ is the set of generalized edges and $\mathcal{T} := \mathcal{T}_{\text{mat}}^\Delta$ is the set of triangles.

Remark 1 a) The subdivision \mathcal{G} can be regarded as a generalization of classical Delaunay triangulations in the sense that disks might assume the classical role of vertices while edges (i.e., objects that connect two neighboring vertices) might

generalize to channels. In the special case of equally sized inclusions such subdivisions have been used in discrete network approximations [3]. Apart from minor technical details regarding the treatment of element boundaries, the subdivision \mathcal{G} fits into the framework of generalized Delaunay partitions for multidimensional sets of convex inclusions introduced in [23].

- b) The subdivision \mathcal{G} covers Ω while the intersection of any two of its elements is of measure zero.
- c) The number of elements in \mathcal{G} is proportional to the cardinality of \mathcal{B} and thus is quasi minimal.
- d) There is a duality concept which links generalized Delaunay triangulations to Voronoi tessellations with respect to the set of disks (see Fig. 2(b) and the next subsection). It generalizes straight-line duality between classical Voronoi tessellation and Delaunay triangulation of point sets. We refer to [23] for more insights about geometric duality and further references.
- e) The generalized Delaunay triangulation \mathcal{D} can be computed fast as explained subsequently. There exist algorithms of order $\mathcal{O}(\#\mathcal{B} \times \log(\#\mathcal{B}))$ for the computation of Voronoi diagrams with respect to a set of disks \mathcal{B} ; see, e.g., [13, 14, 18]. These algorithms, by duality, can also be employed for the computation of the generalized Delaunay subdivision.

We refer to the recent preprint [12] for an algorithmic presentation of this construction.

2.3 Element parametrization and local mesh size

The generalized vertices \mathcal{B}_{inc} and the triangles \mathcal{T} form affine families and can easily be represented by reference elements and affine mappings.

A parametrization of a generalized edge can be given as follows. Let $E = E(B_1, B_2)$ in \mathcal{E} be a generalized edge that connects two generalized vertices $B_1, B_2 \in \mathcal{B}$ and let

$$\Sigma_E := \left\{ y \in \mathbb{R}^2 : \text{dist}(y, B_1) = \text{dist}(y, B_2) \text{ and } \text{dist}(y, B_1) \leq \text{dist}(y, \mathcal{B} \setminus \{B_1, B_2\}) \right\}$$

denote the corresponding dual Voronoi edge, the set of points with equal distance to both B_1 and B_2 . Without loss of generality we assume $r_{B_1} \geq r_{B_2}$, $c_{B_1} = (0, 0)$, $c_{B_2} = (0, \delta)$, $\delta > 0$. Note that the Voronoi dual edge might not be connected (see Fig. 4a). The same applies to the generalized edge as it can be seen in Fig. 4b. We denote the number of connected components of E by $K(E)$. The projection $\pi_{B_1} := \text{argmin}_{y \in B_1} \text{dist}(\cdot, y)$ defines angles

$$-\frac{\pi}{2} \leq \alpha_E^1 \leq \beta_E^1 < \alpha_E^2 \leq \beta_E^2 < \dots < \alpha_E^{K(E)} \leq \beta_{ij}^{K(E)} \leq \frac{\pi}{2}$$

such that

$$\pi_{B_1}(\Sigma_E) = \bigcup_{k=1}^{K(E)} r_{B_1} \left[\sin([\alpha_E^k, \beta_E^k]), \cos([\alpha_E^k, \beta_E^k]) \right]^T.$$

In other words, the parameters $\alpha_E^1, \dots, \alpha_E^{K(E)}, \beta_E^1, \dots, \beta_E^{K(E)}$ are the angular values of the projections of the Voronoi vertices which are connected by Σ_E , onto B_1 . Those Voronoi vertices are simply the circumcenters of triangles adjacent to E . With the reference element

$$E^{\text{ref}} = E^{\text{ref}}(B_1, B_2) := \left(]\alpha_E^1, \beta_E^1[\cup \dots \cup]\alpha_E^{K(E)}, \beta_E^{K(E)}[\right) \times]0, 1[, \quad (2.3)$$

the mapping $J_E : E^{\text{ref}} \rightarrow \text{int}E$, given by

$$\begin{aligned} J_E(s, \lambda) &= (1 - \lambda)r_{B_1} \begin{pmatrix} \sin(s) \\ \cos(s) \end{pmatrix} + \lambda\pi_{B_2} \left((\pi_{B_1}|_{\Sigma_E})^{-1} \left(r_{B_1} \begin{pmatrix} \sin(s) \\ \cos(s) \end{pmatrix} \right) \right) \\ &= \begin{pmatrix} ((1 - \lambda)r_{B_1} + \lambda r_{B_2}) \sin(s) \\ ((1 - \lambda)r_{B_1} - \lambda r_{B_2}) \cos(s) + \delta\lambda \end{pmatrix}, \end{aligned}$$

parametrizes E . Figure 3a visualizes the mapping J_E . Note that a generalized edge $E(B_1, B_2)$ is uniquely determined by the inclusion centers and radii, and the values of α_E , β_E , and δ .

The projection $\pi_{B_1, B_2}(\cdot) := \pi_{B_2}(\pi_{B_1}^{-1}(\cdot))$ may be rewritten as

$$\pi_{B_1, B_2}(x) := \operatorname{argmin}_{y \in \partial B_2} \frac{\operatorname{dist}(x, y)}{\max\{((y - x)/\|y - x\|, \nu_{B_1}(y)), 0\}}, \quad (2.4)$$

where ν_{B_1} denotes the outer normal of B_1 .

With

$$H(s) := \frac{(\delta^2 - 2 \cos(s) \delta r_{B_1}) + r_{B_1}^2 - r_{B_2}^2}{(2 r_{B_2} - 2 r_{B_1}) + 2 \delta \cos(s)}.$$

the parametrization J_E assumes the form

$$\begin{aligned} J_E(s, \lambda) &= \left((1 - \lambda)r_1 + \lambda r_2 \frac{r_{B_1} + H(s)}{r_{B_2} + H(s)} \right) \begin{bmatrix} \sin(s) \\ \cos(s) \end{bmatrix} \\ &\quad + \delta\lambda \left(1 - \frac{r_{B_2}}{r_{B_2} + H(s)} \right) \begin{pmatrix} 0 \\ \delta \end{pmatrix}. \end{aligned} \quad (2.5)$$

We finally introduce some $(\mathcal{T}_{\text{mat}} \cup \mathcal{B})$ -piecewise constant meshsize function $h : \Omega \rightarrow]0, \infty[$ by

$$h|_K = h_K := \operatorname{diam}(K) \quad \text{for } K \in \mathcal{T}_{\text{mat}} \cup \mathcal{B}$$

to be used in the forthcoming finite element analysis. Note that h is not constant with respect to a generalized edge (of positive measure) but captures the distance between neighboring inclusions (see (2.4)).

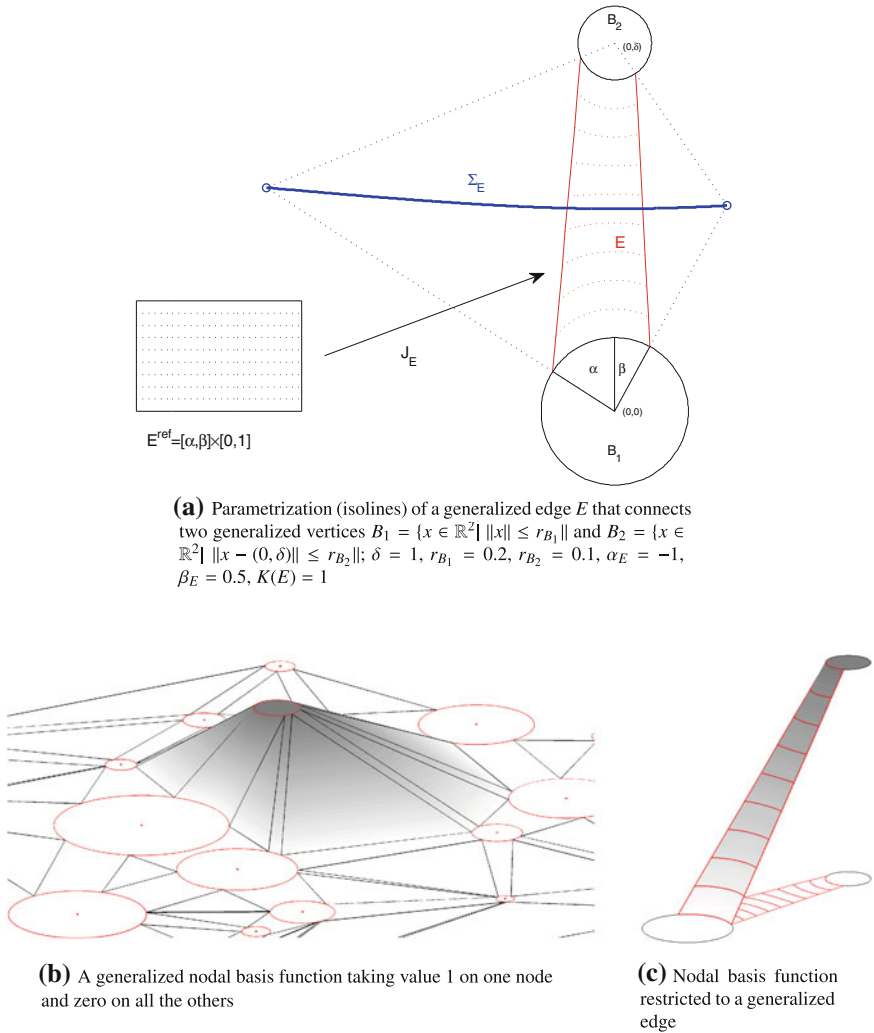


Fig. 3 Edge parametrization and nodal basis function

2.4 Finite element spaces

The degrees of freedom of the finite element spaces are assigned to the entries of \mathcal{B} . Every $B \in \mathcal{B}$ defines a (local) \mathcal{T}_{mat} -affine basis function $\lambda_B : \mathbb{R}^2 \rightarrow [0, 1]$ with

$$\lambda_B \equiv 1 \quad \text{in } B \quad \text{while } \lambda_B \equiv 0 \quad \text{in } \Omega_{\text{inc}} \setminus B.$$

More precisely, λ_B is unique continuous function with constant values on the inclusions as above and whose restriction to each element $T \in \mathcal{T}_{\text{mat}}$ is affine. This means that λ_B is affine on all triangles $T \in \mathcal{T}$. However, λ_B is not affine on generalized edges. Recall

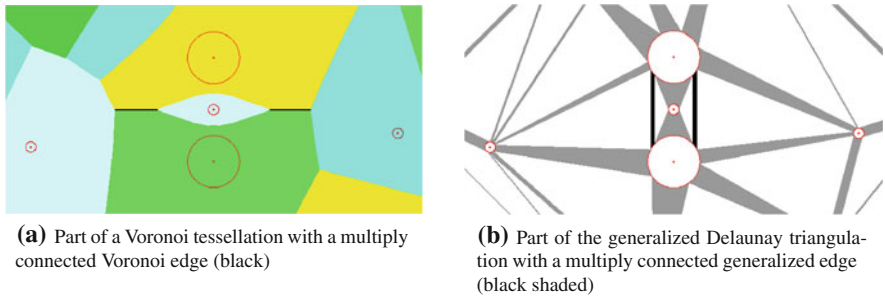


Fig. 4 Voronoi tessellation and Generalized Delaunay triangulation of a set of disks in the plane emphasizing possible non-connectivity of its elements

that a generalized edge $E \in \mathcal{E}$ is the agglomeration of line segments. The restriction of λ_B to all those line segments is supposed to be affine. On the global level of the generalized edge E , this implies that $\lambda_B|_E$ is the image of an affine function on the rectangular reference element E^{ref} (cf. (2.3)) under the coordinate transformation J_E (cf. (2.5)). After suitable rotation of the edge as in Sect. 2.3 (with $B_1 = B$), $\lambda_B|_E$ may be written as

$$\lambda_B(x) = (1 - (J_E^{-1}(x))_2) \text{ for all } x \in E,$$

where $(J_E^{-1}(x))_2$ refers to the second component of the vector $J_E^{-1}(x)$.

Those basis functions generalize nodal basis functions on classical triangular meshes. In the special case of equally sized inclusions, those basis function have been used in the analysis of a network method [4]. The support of λ_B , denoted by ω_B , is given by

$$\omega_B := B \cup (\cup\{E \in \mathcal{E} : E \cap B \neq \emptyset\}) \cup (\cup\{T \in \mathcal{T} : T \cap B \neq \emptyset\}).$$

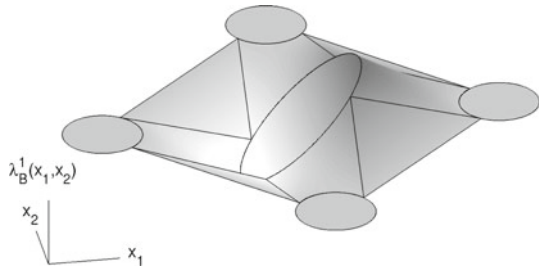
Figure 3b depicts a nodal basis function. Note that the set of nodal basis functions $\Lambda := \{\lambda_B : B \in \mathcal{B}\}$ forms a partition of unity in Ω . The generalized nodal basis functions which are not related to vertices on the Dirichlet boundary Γ_D span the finite element space

$$S^\infty := \text{span}(\Lambda) \cap V. \tag{2.6}$$

Obviously S^∞ has dimension $\#\mathcal{B}$ which is minimal in comparison to data complexity and will be the space of choice for very large contrast and the special case of perfectly conducting inclusions $c_{\text{cont}} = \infty$. In the latter case the solution is necessarily constant with respect to every single inclusion (see Sect. 3.1), which is captured by S^∞ .

If $c_{\text{cont}} < \infty$ then the solution is not constant on the inclusions. Further basis functions (defined below) shall preserve sufficiently high accuracy in this setting, too.

Fig. 5 Basis function λ_B^1



Every $B \in \mathcal{B}_{\text{inc}}$ defines (local) \mathcal{T}_{mat} -affine basis functions $\lambda_B^1, \lambda_B^2 : \mathbb{R}^2 \rightarrow [0, 1]$ with

$$\lambda_B^k(x) = \frac{x_k - (c_B)_k}{r_B} \quad \text{if } x \in B \quad \text{while } \lambda_B^k \equiv 0 \text{ in } \Omega_{\text{inc}} \setminus B.$$

The subscript k refers to the k th component of a 2-dimensional vector.

This means that λ_B^k is affine on all inclusions $B \in \mathcal{B}_{\text{inc}}$ and all triangles $T \in \mathcal{T}$. After suitable rotation of the edge as in Sect. 2.3 (with $B_1 = B$), $\lambda_B|_E$ may be written as

$$\lambda_B^k(x) = (1 - (J_E^{-1}(x))_2)\lambda_B^k(J_E((J_E^{-1}(x))_1, 0)) \quad \text{for all } x \in E,$$

where the coordinate transformation J_E is given in (2.5). Note that $J_E((J_E^{-1}(\cdot))_1, 0) \in \partial B$ and, hence, the values $\lambda_B^k(J_E((J_E^{-1}(\cdot))_1, 0))$ are given by (2.4). It holds $\text{supp}(\lambda_B^k) = \omega_B$. Figure 5 illustrates λ_B^1 .

The enlarged finite element space is then given by

$$S := \text{span}\left(\Lambda \cup \{\lambda_B^1 : B \in \mathcal{B}\} \cup \{\lambda_B^2 : B \in \mathcal{B}_{\text{inc}}\}\right) \cap V. \tag{2.7}$$

Remark 2 a) If the radii of all inclusions are zero, the spaces S resp. S^∞ reduce to the classical conforming \mathbb{P}^1 finite element space with respect to the Delaunay triangulation.

- b) The number of degrees of freedom in S is 3 per inclusion $B \in \mathcal{B}_{\text{inc}}$, and 1 per any other vertex $B \in \mathcal{B}_{\text{mat}}$ away from Γ_D . The overall number of degrees of freedom is bounded by $3\#\mathcal{B}_{\text{inc}} + \#\mathcal{B}_{\text{mat}}$ and, hence, proportional to data complexity.
- c) Further basis functions could easily be designed by considering any continuous function on B and its \mathcal{T}_{mat} -affine or a more general \mathcal{T}_{mat} -polynomial extension to ω_B .

3 Galerkin approximation and a priori error analysis

This section considers the variational formulation of (1.2) and its Galerkin approximation and presents error estimates which are independent of the contrast parameter c_{cont} .

3.1 Variational formulation and solvability

Any minimizer $u^* \in \mathcal{A}$ of (1.2) solves the variational problem

$$\int_{\Omega} c \langle \nabla u^*, \nabla v \rangle dx = \int_{\Omega} f v dx \quad \text{for all } v \in V. \quad (3.1)$$

The left-hand side of (3.1) defines a symmetric bilinear form \mathfrak{a} ,

$$\mathfrak{a}(u, v) := \int_{\Omega} c \langle \nabla u, \nabla v \rangle dx.$$

The sum $u^* := u + u_D$ is the solution of problem (3.1); u_D denotes some extension (with finite energy) of the given inhomogeneous Dirichlet boundary data to Ω . After shifting the inhomogeneous boundary data to the right-hand side, the problem reduces to find $u \in V$ such that

$$\mathfrak{a}(u, v) = \int_{\Omega} f v dx - \mathfrak{a}(u_D, v) =: F(v) \quad \text{for all } v \in V. \quad (3.2)$$

It is obvious that

$$\frac{1}{1 + C_F} \|v\|_{H^1(\Omega)}^2 \leq \mathfrak{a}(v, v) \quad \text{and} \quad \mathfrak{a}(u, v) \leq c_{\text{cont}} \|u\|_{H^1(\Omega)} \|v\|_{H^1(\Omega)} \quad (3.3)$$

for all $u, v \in V$ with the constant from Friedrichs' inequality C_F . Inequality (3.3) ensures the unique solvability of the variational problem (3.2) for finite contrast $c_{\text{cont}} < \infty$.

The Galerkin approximation of the solution of (3.2) with respect to the finite element space S , denoted by $u_S \in S$, is defined as the solution to the discrete variational system

$$\mathfrak{a}(u_S, v) = F(v) \quad \text{for all } v \in S. \quad (3.4)$$

Remark 3 a) The assembling of the corresponding linear system is fairly standard. It might be performed in a loop over all elements of the generalized finite element mesh (including triangles, disks, and edges), the computation of the local stiffness matrices and load vectors, and the sum of the local contributions to the global matrices. The computation of the entries of the local stiffness matrices might be done by transformation to the corresponding reference element. The only difficulty is that the transformation on the generalized edges is not affine. Still the entries of the local stiffness matrices might be precomputed as functions of the angle parameters and δ . Alternatively, numerical quadrature can be used. If two inclusions are close to each other, the basis functions are close to be singular and the quadrature rule should take the singular behavior into account.

b) The resulting stiffness matrix has a similar sparsity pattern as the stiffness matrix of the classical P_1 finite element method for the Poisson problem with respect to some regular triangulation. Hence, in the present 2-dimensional setting, sparse direct solvers offer robust, fast, and parallel solution of the linear system, even though the asymptotic complexity is not optimal (e.g. $\mathcal{O}(N^{3/2})$ for nested dissection [15]). We refer to the textbook [9] for an overview on fast direct solvers for sparse linear systems. For moderate contrast, [1] and [2] show that an iterative solver based on hierarchical factorization performs almost optimal (i.e. $\mathcal{O}(N(\log N)^k)$). In the numerical examples in [1,2], these methods give promising results also in the high contrast regime.

This paper aims at a priori estimates of the error $u - u_S$ in energy norm $\|\cdot\|_a := \sqrt{a(\cdot, \cdot)}$ and therefore estimates of the error in the effective conductivity. Since u_S is the best approximation of u in energy norm we have

$$\begin{aligned} 2(\mathfrak{E}(u_S + u_D) - \mathfrak{E}(u + u_D)) &= \|(u + u_D) - (u_S + u_D)\|_a^2 \\ &= \|u - u_S\|_a^2 = \inf_{v \in S} \|u - v\|_a^2. \end{aligned} \tag{3.5}$$

Sections 3.3 and 3.4 will present bounds of the right hand side in (3.5). A posteriori bounds are presented in [12].

3.2 Perfectly conducting inclusions

Our analysis shall cover the case of perfectly conducting inclusions as well. The related model is a variational problem with respect to the reduced space

$$V^\infty := \{v \in V : v|_B = \text{const} \text{ for all } B \in \mathcal{B}_{\text{inc}}\} \subset V.$$

We seek $u^\infty \in V^\infty$ such that

$$a^\infty(u^\infty, v) = \int_\Omega f v dx - a^\infty(u_D^\infty, v) =: F(v) \text{ for all } v \in V^\infty, \tag{3.6}$$

where $a^\infty(u, v) := \int_{\Omega_{\text{mat}}} \langle \nabla u, \nabla v \rangle dx$ for $u, v \in H^1(\Omega)$ and $u_D^\infty \in H^1(\Omega)$ with $u_D^\infty|_{\Gamma_D} = u_D|_{\Gamma_D}$ and $\nabla u_D^\infty|_B = 0$ for all $B \in \mathcal{B}_{\text{inc}}$.

Since $a^\infty(u, v) \leq \|u\|_{H^1(\Omega)} \|v\|_{H^1(\Omega)}$ and $a^\infty(v, v) = \|\nabla v\|_{L^2(\Omega)}^2$ for all $u, v \in V^\infty$, the variational problem (3.6) has a unique solution.

The Galerkin approximation $u_{S^\infty} \in S^\infty$ of the solution of (3.6), with respect to the finite element space S^∞ defined in (2.6), satisfies

$$a^\infty(u_{S^\infty}, v) = F(v) \text{ for all } v \in S^\infty. \tag{3.7}$$

The error estimate (3.5) remains valid with u replaced by u^∞ and u_S replaced by u_{S^∞} .

Mathematical justification of the limiting problem We shall justify the model problem (3.6). For fixed geometry Ω_{mat} , Dirichlet data $u_D = 0$, and force term f , let $u_{c_{\text{cont}}}$ denote the solution of (3.2) associated with the contrast parameter $c_{\text{cont}} \geq 1$.

Define some function $\tilde{u}_{c_{\text{cont}}} \in V$ as follows. On every $B \in \mathcal{B}_{\text{inc}}$, $(\tilde{u}_{c_{\text{cont}}})|_B$ equals $u_{c_{\text{cont}}}|_B$ minus its mean value $|B|^{-1} \int_B u_{c_{\text{cont}}} dx$. This defines $(\tilde{u}_{c_{\text{cont}}})|_{\Omega_{\text{inc}}}$. Observe that Poincaré’s inequality yields $\|\tilde{u}_{c_{\text{cont}}}\|_{L^2(\Omega_{\text{inc}})} \leq C_1 \|\nabla \tilde{u}_{c_{\text{cont}}}\|_{L^2(\Omega_{\text{inc}})} = C_1 \|\nabla u_{c_{\text{cont}}}\|_{L^2(\Omega_{\text{inc}})}$ with some constant C_1 independent of contrast and the positions of the inclusions. In Ω_{mat} , $\tilde{u}_{c_{\text{cont}}}$ is chosen as some bounded extension of $(\tilde{u}_{c_{\text{cont}}})|_{\Omega_{\text{inc}}}$ in the sense of [26], i.e., there is some constant C_2 that may depend on the geometry but not on c_{cont} such that $\|\tilde{u}_{c_{\text{cont}}}\|_{H^1(\Omega)} \leq C_2 \|u_{c_{\text{cont}}}\|_{H^1(\Omega_{\text{inc}})}$.

This construction and the classical jump relation at the interface $\partial\Omega_{\text{inc}}$,

$$c_{\text{cont}} \frac{\partial ((u_{c_{\text{cont}}})|_{\Omega_{\text{inc}}})}{\partial \nu_{\Omega_{\text{inc}}}} = - \frac{\partial ((u_{c_{\text{cont}}})|_{\Omega_{\text{mat}}})}{\partial \nu_{\Omega_{\text{mat}}}} \quad \text{in } H^{-1/2}(\partial\Omega_{\text{inc}}), \tag{3.8}$$

yield

$$\begin{aligned} & \|\nabla u_{c_{\text{cont}}}\|_{L^2(\Omega_{\text{inc}})} \\ &= \int_{\Omega_{\text{inc}}} \langle \nabla u_{c_{\text{cont}}}, \nabla \tilde{u}_{c_{\text{cont}}}\rangle dx = \int_{\partial\Omega_{\text{inc}}} \frac{\partial u_{c_{\text{cont}}}}{\partial \nu_{\Omega_{\text{inc}}}} \tilde{u}_{c_{\text{cont}}} dx + c_{\text{cont}}^{-1} \int_{\Omega_{\text{inc}}} f \tilde{u}_{c_{\text{cont}}} dx \\ &\leq c_{\text{cont}}^{-1} \left(\left| \int_{\partial\Omega_{\text{mat}}} \frac{\partial u_{c_{\text{cont}}}}{\partial \nu_{\Omega_{\text{mat}}}} \tilde{u}_{c_{\text{cont}}} dx \right| + \|f\|_{L^2(\Omega_{\text{inc}})} \|\tilde{u}_{c_{\text{cont}}}\|_{L^2(\Omega_{\text{inc}})} \right) \\ &\leq c_{\text{cont}}^{-1} (\|\nabla u_{c_{\text{cont}}}\|_{L^2(\Omega_{\text{mat}})} \|\nabla \tilde{u}_{c_{\text{cont}}}\|_{L^2(\Omega_{\text{mat}})} + \|f\|_{L^2(\Omega_{\text{mat}})} \|\tilde{u}_{c_{\text{cont}}}\|_{L^2(\Omega_{\text{mat}})} \\ &\quad + \|f\|_{L^2(\Omega_{\text{inc}})} \|\tilde{u}_{c_{\text{cont}}}\|_{L^2(\Omega_{\text{inc}})}) \\ &\leq C c_{\text{cont}}^{-1} \|f\|_{L^2(\Omega)} \|\nabla u_{c_{\text{cont}}}\|_{L^2(\Omega_{\text{inc}})}, \end{aligned}$$

where C depends only on C_1 and C_2 but not on c_{cont} . This implies

$$\|c^{1/2} \nabla u_{c_{\text{cont}}}\|_{L^2(\Omega_{\text{inc}})} \leq C c_{\text{cont}}^{-1/2} \|f\|_{L^2(\Omega)}.$$

Hence, the solution $u_{c_{\text{cont}}}$ of (3.2) converges (with respect to the energy norm) to the solution u^∞ of (3.6) as $c_{\text{cont}} \rightarrow \infty$.

3.3 Nodal interpolation and approximability

An upper bound for the right-hand side in (3.5) is derived through the design of some finite element function based on a suitable interpolation of the solution u . The conditions

$$\int_B (u - Iu)v dx = 0 \quad \text{for all } v \in \mathbb{P}^1(\mathbb{R}^2) \quad \text{and for all } B \in \mathcal{B}_{\text{inc}}, \tag{3.9a}$$

$$u(b) - Iu(b) = 0 \quad \text{for all } B = \{b\} \in \mathcal{B}_{\text{mat}}, \tag{3.9b}$$

define a generalized nodal interpolation operator $I : H^2(\Omega_{\text{mat}} \cup \Omega_{\text{inc}}) \rightarrow S_0$. Since, on any inclusion $B \in \mathcal{B}_{\text{inc}}$, Iu is the $L^2(B)$ projection of u onto the space of affine functions, we have that

$$\|\nabla^m(u - Iu)\|_{L^2(B)} \leq C_I \text{diam}(B)^{2-m} |u|_{H^2(B)} \quad \text{for } m = 0, 1 \tag{3.10}$$

with some universal constant C_I independent of the diameter of the disk B and $u \in H^2(\Omega_{\text{mat}} \cup \Omega_{\text{inc}})$. The estimate (3.10) already provides approximation properties of the finite element space on the inclusions. It remains to give local estimates for the interpolation error on the triangles (see Lemma 3.1) and the generalized edges (see Lemma 3.3).

As usual, the error on a triangle T depends on the aspect ratio ρ_T , i.e., the ratio between the diameters of the largest circle that can be inscribed in T and the circum-circle of T .

Lemma 3.1 *Let $u \in V \cap H^2(\Omega_{\text{mat}} \cup \Omega_{\text{inc}})$ and let $T \in \mathcal{T}$ with vertices on $B_1, B_2, B_3 \in \mathcal{B}$. Then it holds*

$$\|\nabla(u - Iu)\|_{L^2(T)}^2 \leq C_T^2 \rho_T^{-2} \|h \nabla^2 u\|_{L^2(T \cup B_1 \cup B_2 \cup B_3)}^2 \tag{3.11}$$

with some universal constant C_T which depends only on C_I from (3.9).

Proof A key ingredient of the proof are standard estimates for the interpolation error with respect to a triangle T . It is well known (see [8, Theorem 16.1]) that the nodal (affine) interpolant $I_T u$ of u at the vertices of T satisfies

$$|u - I_T u|_{H^m(T)} \leq C_{\text{ip}} \rho_T^{-1} \text{diam}(T)^{2-m} |u|_{H^2(T)} \quad \text{for all } u \in H^2(T), \quad m = 0, 1. \tag{3.12}$$

The difficulty is that Iu defined by (3.9) does not interpolate u at the vertices of T in general. Thus, the error is split into two components,

$$\|\nabla(u - Iu)\|_{L^2(T)}^2 \leq \|\nabla(u - I_T u)\|_{L^2(T)}^2 + \|\nabla(I_T u - Iu)\|_{L^2(T)}^2. \tag{3.13}$$

The first term on the right-hand side of (3.13) can be estimated directly with (3.12) while the second one requires further considerations.

Notice that $\nabla(I_T u - Iu)|_T$ is constant on T and the inverse estimate

$$\|\nabla q\|_{L^\infty(T)} \leq 2\rho_T^{-1} \text{diam}(T)^{-1} \|q\|_{L^\infty(T)} \tag{3.14}$$

holds for all $q \in \mathbb{P}_1(T)$ on any triangle T . Thus

$$\|\nabla(I_T u - Iu)\|_{L^2(T)}^2 \leq |T| \|\nabla(I_T u - Iu)\|_{L^\infty(T)}^2 \stackrel{(3.14)}{\leq} 4\rho_T^{-2} \|I_T u - Iu\|_{L^\infty(T)}^2. \tag{3.15}$$

The maximal absolute value of the affine function $q := (I_T u - Iu)|_T$ on T is attained in some vertex $x_0 = V(T) \cap B_T$ for some $B_T \in \{B_1, B_2, B_3\}$. If $B_T \in \mathcal{B}_{\text{mat}}$, i.e., $B_T = x_0$, then $(I_T u - Iu)|_T = 0$. Otherwise, let $\tilde{T} \subset B_T$ be the equilateral triangle with vertices on ∂B_T and one vertex at x_0 . For $q \in \mathbb{P}_1(T)$ and $p \in \mathbb{P}_1(\tilde{T})$ with $|p(x_0)| \geq |q(x_0)|$ it holds

$$\|q\|_{L^\infty(T)}^2 = |q(x_0)|^2 \leq |p(x_0)|^2 \leq 2 \left(|\tilde{T}|^{-1} \|p\|_{L^2(\tilde{T})}^2 + \|\nabla p\|_{L^2(\tilde{T})}^2 \right). \tag{3.16}$$

With the special choices $p = (I_T u - Iu)|_T$ and $q = (I_{\tilde{T}} u - Iu)|_{\tilde{T}}$ this leads to

$$\begin{aligned} \|\nabla(I_T u - Iu)\|_{L^2(T)}^2 &\stackrel{(3.15), (3.16)}{\leq} 8\rho_T^{-2} \left(|\tilde{T}|^{-1} \|I_{\tilde{T}} u - Iu\|_{L^2(\tilde{T})}^2 + \|\nabla(I_{\tilde{T}} u - Iu)\|_{L^2(\tilde{T})}^2 \right) \\ &\stackrel{(3.12), (3.10)}{\leq} 16\rho_T^{-2} (C_I^2 + C_{\text{ip}}^2) h_{B_T}^2 \|\nabla^2 u\|_{L^2(B_T)}^2. \end{aligned} \tag{3.17}$$

Together with (3.13) and (3.12) this implies (3.11) with $C_T^2 \leq 5(C_I + C_{\text{ip}})$. □

The second step of the error analysis considers the a priori estimate of the interpolation error on the generalized edges. Every connectivity component E_k , $k = 1, 2, \dots, K(E)$ of an edge $E \in \mathcal{E}$ is a curvilinear polygon, i.e., E_k is a simply-connected, bounded domain with the boundary $\partial E_k = \bigcup_{j=1}^4 \tau_j$, where τ_j are circular arcs. Note that all internal angles $\gamma_1(E_k), \gamma_2(E_k), \dots, \gamma_4(E_k)$ of E_k are bounded from above by $\pi/2$. The subsequent error analysis depends on the smallest angle which is denoted γ_{E_k} . Correspondingly, $\gamma_E := \min_{k=1,2,\dots,K(E)} \gamma_{E_k}$. The following lemma shows that all these angles are bounded from below by a positive constant.

Lemma 3.2 *There exist $\gamma_{\mathcal{E}} > 0$ such that $0 < \gamma_{\mathcal{E}} \leq \gamma_E$ for all $E \in \mathcal{E}$.*

Proof Let $E \in \mathcal{E}$ be some generalized edge connected to the inclusion $B \in \mathcal{B}_{\text{inc}}$. Let τ be one of the straight arcs that define the edge. By design, τ is an element of the infinite Delaunay triangulation \mathcal{T}_{mat} (see Sect. 2.1). Since its circumdisk $CD(\tau)$ is tangential to B (due to the Delaunay criterion (2.1)), τ by itself cannot be tangential to B and the angle between τ and the circular arc $E \cap B$ is necessarily larger than zero.

Lemma 3.3 *Let $u \in V \cap H^2(\Omega_{\text{mat}} \cup \Omega_{\text{inc}})$ and let $E = E(B_1, B_2) \in \mathcal{E}$ be a generalized edge that connects two generalized vertices (inclusions) $B_1, B_2 \in \mathcal{B}_{\text{inc}}$. Then*

$$\|\nabla(u - Iu)\|_{L^2(E)}^2 \leq C_{\mathcal{E}} \left(\|h \nabla^2 u\|_{L^2(E)}^2 + C_E \|h \nabla^2 u\|_{L^2(B_1 \cup B_2)}^2 \right)$$

holds with $C_E := \max_{k=1,2} \|h_{B_k}/h + h/h_{B_k}\|_{L^\infty(E)}$ and some universal constant $C_{\mathcal{E}}$ which depends only on γ_E .

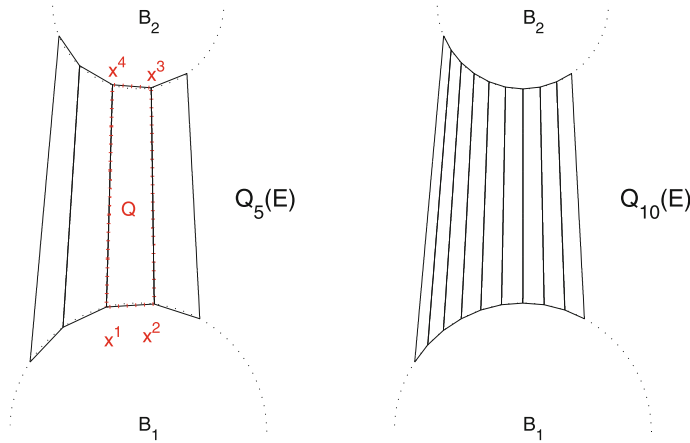


Fig. 6 Subdivisions $Q_5(E)$ and $Q_{10}(E)$ of some generalized edge $E = E(B_1, B_2) \in \mathcal{E}$ into quadrilaterals in the proof of Lemma 3.3

Proof The proof consists of two parts. Part I proves the assertion for $c_{\text{cont}} = \infty$ and prepares the proof in the case $c_{\text{cont}} < \infty$ which is complemented in part II.

Part I. Without loss of generality, let E be connected, $r_{B_1} \geq r_{B_2}$, and $c_{B_1} = 0$, $c_{B_2} = (0, \delta)$ for some $\delta > r_{B_1} + r_{B_2}$. The restriction $E \cap \partial B_1 = \phi([\alpha, \beta])$ of E to B_1 shall be parametrized by some angle $s \in [\alpha, \beta] \subset [-\pi/2, \pi/2]$ with $\phi(s) := r_{B_1}(\sin(s), \cos(s))$. The parameter interval $[\alpha, \beta]$ is subdivided by equidistributed points

$$\alpha = s^1 < s^2 < s^3 < \dots < s^L = \beta.$$

These points are mapped by ϕ onto B_1 and by $\phi \circ \pi_{B_1}$ onto B_2 (recall (2.4) for the definition of π_{B_1}). Let

$$\begin{aligned} \mathcal{Q}_L(E) &:= \{Q_\ell : \ell = 1, \dots, L - 1\} \text{ with} \\ Q_\ell &:= \text{conv}\left(\phi(s^\ell), \phi(s^{\ell+1}), \pi_{B_1}(\phi(s^{\ell+1})), \pi_{B_1}(\phi(s^\ell))\right) \end{aligned}$$

be a subdivision of E into quadrilaterals (see Fig. 6).

The union of quadrilaterals on level L provides a polygonal approximation $E^L := \bigcup_{Q \in \mathcal{Q}_L(E)} Q$ of $E \subset E^L \subset \text{conv}(E)$ for all L with $|E^L \setminus E| \rightarrow 0$ as $L \rightarrow \infty$. A (bounded) extension operator $(\cdot)_E : H^2(E) \rightarrow H^2(\mathbb{R}^d)$ (see, e.g., [26]) extends $u|_E$ to $\text{conv}(E)$. The extended function is denoted by u_E .

The nodal (bilinear) interpolation operator with respect to $Q \in \mathcal{Q}_L$ is denoted by J_Q and its \mathcal{Q}_L -piecewise version by $J_{\mathcal{Q}_L}$. Theorem 3.8 from [22] implies

$$\|\nabla(u_E - J_{\mathcal{Q}_L}u_E)\|_{L^2(Q)} \leq C_Q \text{diam}(Q) \|\nabla^2 u_E\|_{L^2(Q)} \tag{3.18}$$

for all $Q \in \mathcal{Q}_L$, $L \in \mathbb{N}$. The constant C_Q depends only on the interior angles of Q , i.e., C_Q can be bounded uniformly for all $Q \in \mathcal{Q}_L$ and all $L \in \mathbb{N}$ in terms of γ_E . Thus

$$\begin{aligned} \|\nabla(u_E - J_{\mathcal{Q}_L}u_E)\|_{L^2(E^L)}^2 &= \sum_{Q \in \mathcal{Q}_L} \|\nabla(u_E - J_Q u_E)\|_{L^2(Q)}^2 \\ &\stackrel{(3.18)}{\leq} \sum_{Q \in \mathcal{Q}_L} C_1 \|\text{diam}(Q)\nabla^2 u_E\|_{L^2(Q)}^2 \end{aligned} \tag{3.19}$$

with some constant C_1 which depends only on γ_E . Let L tend to infinity in (3.19) to verify

$$\|\nabla(u - \tilde{u})\|_{L^2(E)}^2 \leq C_1 \|h\nabla^2 u\|_{L^2(E)}^2 \tag{3.20}$$

for $\tilde{u} := \lim_{L \rightarrow \infty} J_{\mathcal{Q}_L}u_E$. If $c_{\text{cont}} = \infty$ then $\tilde{u} = Iu$ and the proof is finished.

Part II. If otherwise $c_{\text{cont}} < \infty$ then, in general, $\tilde{u} \notin S$ and $\|\nabla(Iu - \tilde{u})\|_{L^2(E)}$ needs to be estimated further. The sequence $e_L := J_{\mathcal{Q}_L}(Iu)_E - J_{\mathcal{Q}_L}u_E$ converges (in H^1) to $e := Iu - \tilde{u}$ as $L \rightarrow \infty$. Thus, bounds on $\|\nabla e_L\|_{L^2(E^L)}$ will lead to a bound on $\|\nabla(Iu - \tilde{u})\|_{L^2(E)}$. Let $Q \in \mathcal{Q}_L$ with

$$\partial Q = [x^1, x^2] \cup [x^2, x^3] \cup [x^3, x^4] \cup [x^4, x^1]$$

and $x^1, x^2 \in B_1$ and $x^3, x^4 \in B_2$ and $x^5 = x^1$ as in Fig. 6 (left). The vector $\nabla e_L|_Q$ is written as some linear combination of the vectors $(x^{k+1} - x^k)/|x^{k+1} - x^k|$ such that

$$\|\nabla e_L\|_{L^2(Q)}^2 \leq |Q| \|\nabla e_L\|_{L^\infty(Q)}^2 \leq C_2 |Q| \sum_{k=1}^4 \frac{|\langle (\nabla e_L)|_{[x^k, x^{k+1}]}, x^{k+1} - x^k \rangle|^2}{|x^{k+1} - x^k|^2}$$

with a constant C_2 which depends only on the maximal angle in Q and can be bounded uniformly in terms of γ_E^{-1} . Using $\langle (\nabla e_L)|_{[x^k, x^{k+1}]}, x^{k+1} - x^k \rangle = e_L(x^{k+1}) - e_L(x^k)$ for $k = 2$ and $k = 4$, this yields

$$\begin{aligned} \|\nabla e_L\|_{L^2(Q)}^2 &\leq C_2 \left(\|h\|_{L^\infty(Q)} \|\nabla e_L\|_{L^2([x^1, x^2] \cup [x^3, x^4])}^2 \right. \\ &\quad \left. + \|h^{-1}\|_{L^\infty(Q)} \|e\|_{L^2([x^2, x^3] \cup [x^4, x^1])}^2 \right). \end{aligned} \tag{3.21}$$

The summation of (3.21) over $Q \in \mathcal{Q}_L$ leads to

$$\begin{aligned} \|\nabla e_L\|_{L^2(E^L)}^2 &\leq C_2 \left(\|h\|_{L^\infty(E)} \|\nabla e_L\|_{L^2(\partial E_L \cap (B_1 \cup B_2))}^2 \right. \\ &\quad \left. + \|h^{-1}\|_{L^\infty(E)} \|e_L\|_{L^2(\partial E_L \cap (B_1 \cup B_2))}^2 \right). \end{aligned}$$

In the limit $L \rightarrow \infty$ it follows

$$\|\nabla e\|_{L^2(E)}^2 \leq C_2 \left(\|h\|_{L^\infty(Q)} \|\nabla e\|_{L^2(\partial E \cap (B_1 \cup B_2))}^2 + \|h^{-1}\|_{L^\infty(Q)} \|e\|_{L^2(\partial E \cap (B_1 \cup B_2))}^2 \right). \tag{3.22}$$

Estimate (3.10) and the trace inequality

$$\|f\|_{L^2(\partial B)} \leq \sqrt[4]{8} \left(\|f\|_{L^2(B)} + \|f\|_{L^2(B)}^{1/2} \|\nabla f\|_{L^2(B)}^{1/2} \right), \tag{3.23}$$

valid for any disk B and $f \in H^1(B)$ (see [6, Proposition 1.6.3]), imply

$$\begin{aligned} |e|_{H^m(\partial B)} &= |\tilde{u} - Iu|_{H^m(\partial B)} = |u - Iu|_{H^m(\partial B)} \\ &\stackrel{(3.23), (3.10)}{\leq} \sqrt[4]{8} C_I r_B^{2-m-\frac{1}{2}} |u|_{H^2(B)} \text{ for } m = 0, 1. \end{aligned} \tag{3.24}$$

With a universal constant C_3 which depends only on C_I and γ_E (through C_1 and C_2), this leads to

$$\|\nabla(Iu - \tilde{u})\|_{L^2(E)}^2 \stackrel{(3.21), (3.24)}{\leq} C_3 \|h^{-1}(h|_{B_k}) + h(h|_{B_k})^{-1}\|_{L^\infty(E)} \|h\nabla^2 u\|_{H^2(B_1 \cup B_2)}^2.$$

This concludes the proof of the lemma. □

The constant C_E reflects the fact that two inclusions might touch but the corresponding affine approximations of the solution on the disks might not match at the touching point. Thus, in rare cases for $c_{\text{cont}} < \infty$, the discrete system might have infinite energy whereas the continuous solution has not. Choosing sufficiently many degrees of freedom (number of degrees of freedom per inclusion larger than or equal to the number of neighbors per inclusion) this problem disappears.

3.4 A priori error estimates

The approximation property of the finite element space S reads as follows.

Theorem 3.1 *Let $u \in V \cap H^2(\Omega_{\text{mat}} \cup \Omega_{\text{inc}})$ be the solution of (3.2) and let $u_S \in S$ be its Galerkin approximation that solves (3.4). Then it holds*

$$\|u - u_S\|_{\mathfrak{a}}^2 \leq C_S^2 \left(\|h\nabla^2 u\|_{L^2(\Omega_{\text{mat}})}^2 + c_{\text{cont}} \sum_{B \in \mathcal{B}_{\text{inc}}} C_B \|h\nabla^2 u\|_{L^2(B)}^2 \right)$$

with $C_B := \|h_B/h + h/h_B\|_{L^\infty(\omega_B)}$ and some universal constant C_S which depends only on C_I , C_T , and C_E .

Proof The proof is a straight forward consequence of (3.10), Lemma 3.1, Lemma 3.3, and the equality

$$\|v\|_{\alpha}^2 = \|\nabla v\|_{L^2(\Omega_{\text{mat}})}^2 + c_{\text{cont}} \|\nabla v\|_{L^2(\Omega_{\text{inc}})}^2 \quad \text{for all } v \in H^1(\Omega).$$

□

By (3.3) the estimate of Theorem 3.1 is also valid for the error measured in the $H^1(\Omega)$ -norm. The regularity results from [7, Appendix B] read

$$\|\nabla^2 u\|_{L^2(\Omega_{\text{mat}})} \leq C_{\text{reg}} \|f\|_{L^2(\Omega)}, \quad \|\nabla^2 u\|_{L^2(\Omega_{\text{inc}})} \leq \frac{C_{\text{reg}}}{c_{\text{cont}}} \|f\|_{L^2(\Omega)}. \quad (3.25)$$

The constant C_{reg} depends solely on the geometry of the set inclusions and Ω but *not* on c_{cont} . This implies that the contrast is not a critical parameter.

Corollary 3.1 *Let $u \in V \cap H^2(\Omega_{\text{mat}} \cup \Omega_{\text{inc}})$ be the solution of (3.2) and $u_S \in S$ its Galerkin approximation that solves (3.4). Then it holds*

$$\|u - u_S\|_{\alpha} \leq \tilde{C}_S \|h\|_{L^\infty(\Omega)} (\|f\|_{L^2(\Omega)} + \|\nabla u_D\|_{L^2(\Omega)}) \quad (3.26)$$

with some universal constant \tilde{C}_S which depends only on C_{reg} and the constants C_S, C_B from Theorem 3.1.

The constant \tilde{C}_S in (3.26) does not depend on the contrast parameter $c_{\text{cont}} > 1$. However, through the constants C_B , it might depend on the term (cf. the Definition of C_B in Theorem 3.1)

$$\max_{E(B_1, B_2) \in \mathcal{E}} \frac{\max\{r_{B_1}, r_{B_2}\}}{\text{dist}(B_1, B_2) c_{\text{cont}}}. \quad (3.27)$$

The latter constant is critical with regard to the geometry of the coefficient function. The term may blow up, whenever the distance of two inclusions relative to their size becomes very small. However, high contrast reduces this effect. In the case of perfectly conducting inclusions ($c_{\text{cont}} = \infty$) it even disappears. The generalized interpolation operator from (3.9) fulfills $(u - Iu)|_B = 0$ for all $B \in \mathcal{B}$ and the proof of Lemma 3.3 consists only of part I. Lemma 3.1 can be simplified in a similar way which leads to the following corollary.

Corollary 3.2 *Let $c_{\text{cont}} = \infty$ and let $u^\infty \in V^\infty \cap H^2(\Omega_{\text{mat}} \cup \Omega_{\text{inc}})$ be the solution of (3.6) and $u_{S^\infty} \in S^\infty$ its Galerkin approximation that solves (3.7). Then it holds*

$$\|\nabla(u^\infty - u_{S^\infty})\|_{L^2(\Omega)} = \|u^\infty - u_{S^\infty}\|_{\alpha} \leq C_{S^\infty} \|h\| \|\nabla^2 u^\infty\|_{L^2(\Omega_{\text{mat}})}$$

with a constant C_{S^∞} independent of $u^\infty, c_{\text{cont}}$, and the location of the inclusions.

In the general case $c_{\text{cont}} < \infty$ the critical constant shown in (3.27) can easily be reduced with higher-order ansatz functions on the inclusions. We can therefore derive error estimates whose constants are explicit in the underlying geometry. However, in all cases the dependence on the H^2 -norm of the solution remains. This issue is briefly discussed in the Sect. 4.3.

4 Concluding remarks

The main result of this paper is a numerical scheme to compute temperature distributions in composite materials with a large number of particles and high contrast. In the model situation under consideration, the method is robust and does *not* depend on the contrast $c_{\text{cont}} \rightarrow \infty$. Some of the results extend to a more general geometric setting in a straight-forward way. However, some difficulties remain open.

4.1 General inclusion geometry

For the use in practical applications it is desirable to incorporate more general inclusion shapes and 3-dimensional geometries. It is shown in [23] that the generalized partitions of Sect. 2 nicely generalize to sets of convex inclusions, e.g., ellipsoids, convex polyhedra, and line segments. Even more, the design allows inclusions to intersect. Thus, generalized Delaunay triangulations are also available for non-convex inclusions which can be represented by finite unions of convex ones. The design of according finite element methods can be done similarly as presented here. However, the complexity of the mesh and the corresponding finite element method will grow as the number of shape parameters that define a single inclusion grows. For smooth inclusions the corresponding analysis is straight-forward; non-smooth inclusions, however, require new arguments which are able to cope with lack of regularity.

4.2 Convergence

By straight forward arguments it is easy to show that the finite element solutions (the solutions of (3.2) and (3.6)) converge in H^1 to the solution of (1.2) if the meshwidth function h tends to 0.

In the matrix, the meshwidth function h can be decreased in the matrix Ω_{mat} by simply putting additional artificial inclusions (points) in the set \mathcal{B}_{mat} . If $c_{\text{cont}} = \infty$, this suffices to be able to construct a convergent sequence of approximation because the (energy-)error in the inclusions is always zero. The case, in which additional vertices of radius zero are added to improve the approximability properties of the finite element space, is already treated by the theory presented in this article. A different possibility is to leave the initial partition as it is and increase the polynomial degree of the shape functions. This strategy, the so-called p -refinement, is recommended for problems where geometry and data are smooth. The definition of higher-order finite element spaces is to some extent straight-forward, the corresponding analysis, however, appears more involved.

If $c_{\text{cont}} < \infty$, in addition, the error on the inclusions has to be decreased, e.g., by increasing the polynomial degree.

4.3 Geometry-explicit estimates

The method presented is stable with respect to contrast in the medium. However, the error bounds might depend on geometric parameters of the material, e.g., the distance between neighboring particles. Whether or not the dependence on the local distance is critical depends on the global distribution of particles. This can be seen already in the simplified situation of perfectly conducting ($c_{\text{cont}} = \infty$) inclusions.

Consider first two inclusions that touch but are isolated from further inclusions. Since the solution is found in H^1 the (constant) values of the solution on the two inclusions have to be equal. Provided the force term is sufficiently smooth (L^2), classical regularity theory ensures smoothness of the solution in some neighborhood of the two inclusions and the constant in the regularity estimate depends only on the distance to further inclusions or the boundary of the domain.

The critical scenario is the appearance of an almost conducting path of inclusions which connects two parts of the outer boundary with different, prescribed temperature. The temperature gap needs to be compensated in the small regions between the inclusions of the path which might cause steep gradients in the solution. If the inclusions of the path touch pairwise, the path is perfectly conducting and hence, the energy is infinite. Depending on the volume fraction of particles, the material shows a phase transition from moderate to high conductivity. Mathematically speaking, the solution operator, which maps a pair the data u_D and f to the solution of (1.2), is not uniformly bounded with respect to the geometry of the set of inclusions \mathcal{I} [25, Theorem 3.5] shows that, though the energy of the solution might blow up, the error estimate in Corollary 3.2 is bounded by some generic constant independent of the distance of the particles. Thus, our method is robust with respect the such critical scenarios and allows meaningful material simulation even in densely packed composites. We refer to [12] for numerical experiments.

In the general case of high but finite contrast the situation appears more involved and a corresponding regularity theory that is explicit (and sharp) with respect to both, contrast and geometric parameters, is not yet available and has to be addressed in future research.

References

1. Bebendorf, M.: Why finite element discretizations can be factored by triangular hierarchical matrices. *SIAM J. Numer. Anal.* **45**(4), 1472–1494 (2007)
2. Börm, S.: Approximation of solution operators of elliptic partial differential equations by \mathcal{H} - and \mathcal{H}^2 -matrices. *Numer. Math.* **115**(2), 165–193 (2010)
3. Berlyand, L., Kolpakov, A.: Network approximation in the limit of small interparticle distance of the effective properties of a high-contrast random dispersed composite. *Arch. Ration. Mech. Anal.* **159**(3), 179–227 (2001)
4. Berlyand, L., Novikov, A.: Error of the network approximation for densely packed composites with irregular geometry. *SIAM J. Math. Anal.* **34**(2), 385–408 (2002) (electronic)
5. Borcea, L., Papanicolaou, G.C.: Network approximation for transport properties of high contrast materials. *SIAM J. Appl. Math.* **58**, 501–539 (1998)
6. Brenner, S.C., Scott, L.R.: The mathematical theory of finite element methods. In: *Texts in Applied Mathematics*, 3rd edn, vol. 15. Springer, New York (2008)

7. Chu, C.-C., Graham, I.G., Hou, T.Y.: A new multiscale finite element method for high-contrast elliptic interface problems. *Math. Comput.* **79**, 1915–1955 (2010)
8. Ciarlet, P.: *The Finite Element Method for Elliptic Problems*. North Holland, Amsterdam (1978)
9. Davis, T.A.: *Direct methods for sparse linear systems*. In: *Fundamentals of Algorithms*, vol. 2. Society for Industrial and Applied Mathematics (SIAM), Philadelphia (2006)
10. Delaunay, B.: Sur la sphère vide. *Izvestia Akademii Nauk SSSR, Otdelenie Matematicheskikh i Estestvennykh Nauk* **7**, 793–800 (1934)
11. Weinan, E., Engquist, B.: The heterogeneous multiscale methods. *Commun. Math. Sci.* **1**(1), 87–132 (2003)
12. Eigel, M., Peterseim, D.: *Network FEM for Composite Materials with A Posteriori Control* DFG Research Center Matheon Berlin, Preprint Series, vol. 985 (2012)
13. Fortune, S.: A sweepline algorithm for Voronoi diagrams. *Algorithmica* **2**(2), 153–174 (1987)
14. Gavrilova, M., Rokne, J.: Swap conditions for dynamic Voronoi diagrams for circles and line segments. *Comput. Aided Geom. Design* **16**(2), 89–106 (1999)
15. George, A., Liu, J.: *Computer Solution of Large Sparse Positive Definite Systems*. Prentice-Hall, Englewood Cliffs (1981)
16. Hou, T.Y., Wu, X.-H.: A multiscale finite element method for elliptic problems in composite materials and porous media. *J. Comput. Phys.* **134**, 169–189 (1997)
17. Hughes, T.J.R., Feijóo, G.R., Mazzei, L., Quincy, J.-B.: The variational multiscale method—a paradigm for computational mechanics. *Comput. Methods Appl. Mech. Eng.* **166**(1–2), 3–24 (1998)
18. Kim, D.-S., Kim, D., Sugihara, K.: Voronoi diagram of a circle set from Voronoi diagram of a point set. I. *Topology. Comput. Aided Geom. Design* **18**(6), 541–562 (2001)
19. Kolpakov, A.A., Kolpakov, A.G.: *Capacity and transport in contrast composite structures*. CRC Press, Boca Raton (2010)
20. Larson, M.G., Målqvist, A.: Adaptive variational multiscale methods based on a posteriori error estimation: energy norm estimates for elliptic problems. *Comput. Methods Appl. Mech. Eng.* **196**(21–24), 2313–2324 (2007)
21. Målqvist, A., Peterseim, D.: *Localization of Elliptic Multiscale Problems*. ArXiv e-prints, 1110.0692 (2011)
22. Mao, S., Nicaise, S., Shi, Z.-C.: On the interpolation error estimates for Q_1 quadrilateral finite elements. *SIAM J. Numer. Anal.* **47**(1), 467–486 (2008)
23. Peterseim, D.: *Generalized Delaunay partitions and composite material modeling*. DFG Research Center Matheon Berlin, Preprint Series, vol. 690 (2010)
24. Peterseim, D.: Triangulating a system of disks. In: *Proceedings of the EuroCG 2010*. Dortmund, Germany (2010)
25. Peterseim, D.: Robustness of Finite Element Simulations in Densely Packed Random Particle Composites. *Netw. Heterog Media* **7**(1), 113–126 (2012)
26. Stein, E.M.: *Singular Integrals and Differentiability Properties of Function*. Princeton Univ. Press, New York (1970)
27. Voronoi, G.F.: Nouvelles applications des paramètres continus à la théorie des formes quadratiques. *Journal für die Reine und Angewandte Mathematik* **133**, 97–178 (1907)